RSC Advances

PAPER

View Article Online
View Journal | View Issue

Cite this: *RSC Adv.*, 2021, **11**, 18509

Multifunctional carbon-supported bioactive hybrid nanocomposite (C/GO/NCP) bed for superior water decontamination from waterborne microorganisms†

Michał Jakubczak, *[a] Ewa Karwowska,[b] Alicja Fiedorczuk[b] and Agnieszka M. Jastrzębska[a]

Achieving both effective and sustainable water decontamination technology requires development of a universal filtration solution. However, effective removal of natural waterborne microorganisms still remains a challenge. The use of nanoparticles in water filters is promising but also leads to problems with their efficiency and safety. To cross these bottlenecks, we have designed a novel multifunctional carbon-supported bioactive hybrid nanocomposite filtration bed. For this purpose, we took advantage of granular activated carbon (C), graphene oxide (GO) and bioactive Al_2O_3/Ag nanocomposite particles (NCP). These components were assembled into a hybrid nanocomposite structure using facile *in situ* surface decoration *via* a sol–gel approach. This obtained C/GO/NCP filtration bed was thoroughly characterized in terms of morphology, structure and surface properties as well as further evaluated for tap water filtration efficiency. Analysis of the preferential sites for bacteria adsorption and biological tests under close-to-real static and dynamic filtration conditions has proved C/GO/NCP's efficiency in eliminating model and natural strains of waterborne microorganisms. At the same time, nanoparticles were not released into the filtrate, which confirmed material stability and safety. We have also revealed that C/GO/NCP nanofiltration bed was self-sterilizing which means that it entirely eliminated up to 100% of the filtered bacteria cells within short periods of contact time. What is more, the low-temperature thermal regeneration allowed recovering the assumed properties. In general, the obtained results indicate a breakthrough in designing hybrid-structured filtration beds that can be easily synthesized and safely used for drinking water decontamination.

Received 24th March 2021
Accepted 17th May 2021

DOI: 10.1039/d1ra02315b

rsc.li/rsc-advances

1 Introduction

Sustainable production of clean drinking water poses a challenge for developing countries. Therefore, polluted surface and ground waters are constantly being used for everyday life.[1] In 2017, at least 2 billion people used water sources contaminated with faeces that readily transmitted diseases such as diarrhea, cholera, dysentery, typhoid, or even polio.[2] In general, the use of contaminated tap water sources is estimated to cause at least 485 000 diarrhoeal deaths per year.[3] The contamination may be caused by physical, chemical and microbiological agents such as bacteria, protozoa, viruses, and parasites.[4] Their presence in tap water is related to deficiencies or even a lack of sanitary infrastructure.[5] Consequently, since 1892, *Escherichia coli* bacteria remains the primary indicator of water fecal contamination.[1,6,7]

The aforementioned problems may be solved by the use of advanced water treatment technologies. Unfortunately, their application in third-world countries is hindered because of the required developed infrastructure. Therefore, the point-of-use filtration technologies can be promising in such places because their successful application accounts for the interplay of simplicity and efficiency.[8] It is likely that the most universal and efficient filtration system may require using nano-technological solutions.[9] Nanomaterials are excellent adsorbents, catalysts and biosensors.[5,6,10–12] Their bactericidal and bacteriostatic properties are known for many years too.[10,13,14] Consequently, they can be involved in removal of various types of waterborne microorganisms.

Activated carbons (C) and their granular counterparts are widely used in traditional and novel filtration systems because of their nonspecific activity in removing both inorganic and organic matter.[15,16] Recently, an emphasis is given to modify carbons with nanosilver (Ag) to enable more specific removal of bio-

[a]*Warsaw University of Technology, Faculty of Materials Science and Engineering, Wołoska 141, 02-507 Warsaw, Poland. E-mail: michal.jakubczak.dokt@pw.edu.pl; agnieszka.jastrzebska@pw.edu.pl; Tel: +48-22-234-7449*

[b]*Warsaw University of Technology, Faculty of Building Services, Hydro and Environmental Engineering, Nowowiejska 20, 00-653 Warsaw, Poland. E-mail: ewa.karwowska@pw.edu.pl; ala.fiedorczuk@gmail.com*

† Electronic supplementary information (ESI) available. See DOI: 10.1039/d1ra02315b

contaminants. Ag-impregnated granular activated carbons (C/Ag) gained a lot of attention in point-of-use (POU) cleaning of tap water for drinking and domestic use because of good disinfecting properties[17] against, for instance, *E. coli* bacteria.[18] Other solutions involved ceramic disks,[19] anion resin, zeolite, sand and fibreglass filtration beds[20] coated with Ag nanoparticles. These were effective against microbiological contamination but caused a release of nanosilver into the filtrate.[19] In other approaches, they were not tested in flow-type systems.[18] Even though some nanomaterials were effective against *E. coli*, *S. typhimurium*, *S. dysenteriae* and *V. cholerae* bacteria,[20] only the anion resin bead showed sufficient stability.[20]

Our recent studies have shown that it is possible to obtain interesting biological properties of graphene family materials by anchoring graphene oxide (GO) or reduced graphene oxide (RGO) with ceramic oxide, and noble metals.[21] We proved that RGO/Al_2O_3-M (where M = Ag, Au, or Pd) nanostructures are efficient adsorbents for bacteria cells such as *E. coli*, *S. aureus*, *Bacillus* sp., and *Sarcina* sp. The best application potential for water filtration showed RGO/Al_2O_3/Ag nanocomposite. It was both biocidal and biosorptive due to the electrostatic attraction of bacterial cells.[22] The follow-up study compared the bioactivity of RGO/Me_xO_y–Ag (where Me_xO_y = Al_2O_3, TiO_2, SiO_2 or ZnO_2) structures and proved that the presence of Me_xO_y in nanocomposite provides a specific matrix for the internally embedded Ag nanoparticles.[23] What is more, by choosing the appropriate ceramic oxide for anchoring Ag nanoparticles to RGO surface, it is possible to control the efficiency of the nanocomposite.[24] It is worth noting that the studies involved *in situ* reduction of GO to RGO *via* a chemical reaction between metal alkoxide and terminal functional –OH groups present at theGO surface. Finally, we have revealed that Al_2O_3 is present in bactericidal RGO/Al_2O_3–Ag nanocomposite as an amorphous, highly porous layer covalently bonded to GO surface.[21,25]

This study explores an application potential of a novel multifunctional carbon-supported bioactive hybrid nanocomposite filtration bed (see Fig. 1). The work aimed at designing the most efficient nano-composition, obtaining it *via* one-pot approach with zero-waste, and examination to how extend surface modification of activated carbon (C) with graphene oxide (GO) and bioactive Al_2O_3/Ag nanocomposite particles (NCP) enhances material's biological activity and water decontamination efficiency. We have carried out the filtration process in static and dynamic close-to-real conditions, which involved tests on both model and natural waterborne microorganisms. Moreover, to check if the adsorptive properties are somewhat specific to the type of bacteria strain and/or affects the surface-adsorption efficiency, we have used simulated mixtures of *coccobacillus* and *staphylococci* cells. The results showed the superior activity of the designed C/GO/NCP in water decontamination from waterborne bacteria.

2 Materials and methods

2.1. Synthesis of the C/GO/NCP filtration bed

The granular activated carbon (C), graphene oxide (GO), and bioactive Al_2O_3/Ag nanocomposite particles (NCP) were assembled into a hybrid nanocomposite structure using facile *in situ* zero-waste surface decoration *via* one-pot sol–gel approach. The procedure of C/GO/NCP's synthesis can be described as follows: the 150 cm^3 reactor equipped with a magnetic stirrer was filled with 100 cm^3 of isopropanol and added with 0.01 g of GO flakes. The mixture was subsequently homogenized for 1 minute in the periodical working mode (1 s work/1 s brake) using a Sonics Vibra-Cell ultrasonic homogenizer. Next, 0.2 g of aluminum triisopropoxide was added and the reaction mixture was stirred for 30 minutes with 200 rpm. Subsequently, 20 cm^3 of separately prepared silver acetate water solution (0.09 g/20 cm^3) was added to the GO-containing mixture and the stirring process was continued for additional 15 minutes. In a final step, 9.78463 g of activated carbon was soaked in 50 cm^3 of isopropanol and then added to the main reaction mixture followed by stirring for 30 minutes with 200 rpm. After this time, the mixture was poured into the flat crystallizer and left overnight at 25 °C to let the solvent fully evaporate. The reference sample of C/Al_2O_3/Ag was prepared using the abovementioned approach and by skipping the middle step of GO addition to the reaction mixture. After drying, the samples were calcinated at 300 °C for 1 hour in a muffle furnace. The temperature was chosen based on our previous research.[26]

Chemical reagents used in the synthesis (isopropanol, ethyl alcohol, aluminum triisopropoxide and silver lactate) were purchased from Sigma Aldrich (Gillingham, Dorset, UK) and used as received. Graphene oxide (GO) flakes were received from the Institute of Electronic Materials Technology (Wólczyńska 133, 01-919 Warszawa, Poland) and were synthesized from natural graphite flakes using the modified Hummer's method. The sample of granular activated carbon widely used in the commercial POU systems was obtained from the UST-M Sp. z o.o. Company (Piaskowa 124A, 97-200 Tomaszów Mazowiecki, Poland).

2.2. Characterization of the morphology and structure

Analysis of C/GO/NCP's morphology and the structure was carried out at an accelerating voltage from 3.0 to 15.0 kV using LEO 1530 (Zeiss, USA) scanning electron microscope (SEM). Before analysis, samples were directly spread on the surface of the sticky carbon tape and then coated with a thin carbon layer using a BAL-TEC SCD 005 sputter coater.

2.3. Analysis of physical properties and porous structure

The physical properties and porous structure of the samples were analyzed using the physical nitrogen sorption method, using the Quadrasorb-SI (Quantachrome Instruments, Germany) equipped with Flo Vac degasser. The adsorption and desorption process was carried out in a liquid nitrogen bath at −195 °C. The Brunauer–Emmet–Teller method (BET) was used to determine the specific surface area (S_{BET}). The total pore volume (V_{pore}) and average pore size (D_{pore}) parameters were analyzed using the Barret–Joyner–Halend (BJH) method.

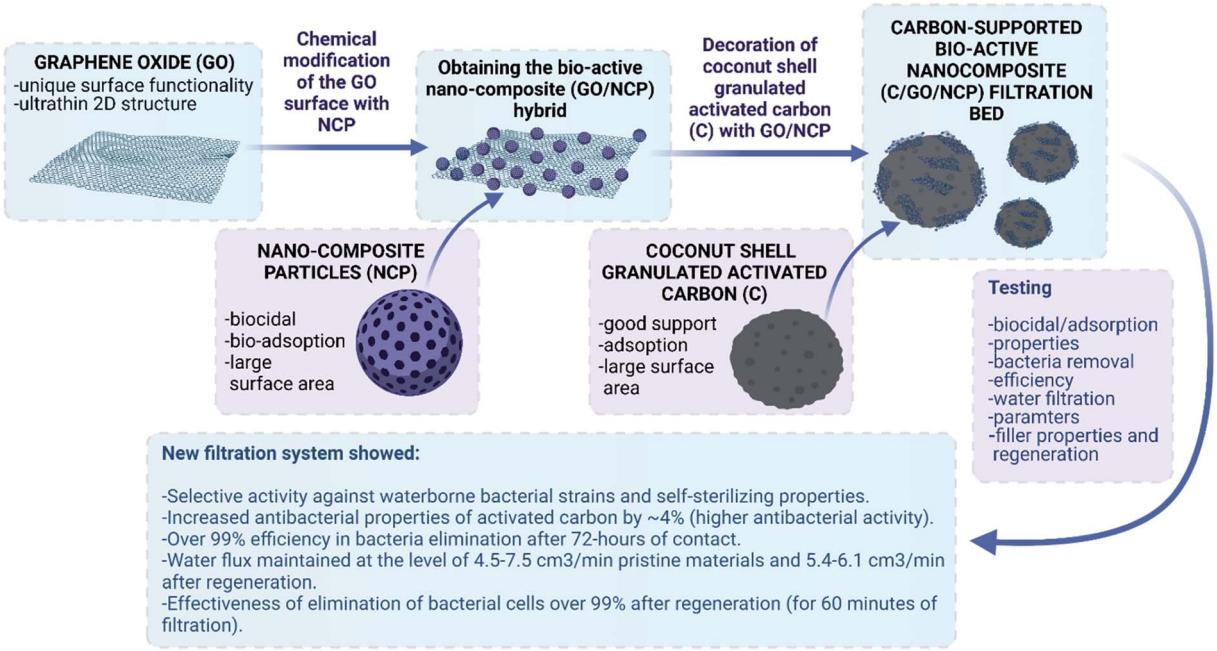

Fig. 1 Schematic presentation of research approach and expected feasibility.

2.4. Preparation of the model bacterial strains

Model bacteria strains were prepared as follows: the *Escherichia coli*, *Staphylococcus aureus*, *Bacillus* sp. bacterial strains, obtained from the private collection of the Biology Department, Faculty of Building Services, Hydro and Environmental Engineering, Warsaw University of Technology, were cultured on an agar medium (Merck, USA) in Petri dishes for 24 hours at 37 °C.

2.5. Preparation of the waterborne bacterial strains isolated from the natural environment

Waterborne bacterial strains were isolated from surface water samples. Microorganisms were cultured on a standard nutrient agar medium (Nutrient LAB-AGAR™, Biocorp) for 48 hours at 26 °C. Pure bacteria strains were obtained using the reduction culturing technique and as such, were used for further studies.

2.6. Analysis of preferential sites for bacteria adsorption

The qualitative analysis of preferential sites for adsorption of bacteria cells (*coccobacillus* and *staphylococci* bacteria mixtures) on the sample's surface was investigated using scanning electron microscope LEO 1530 (Zeiss, USA) at an accelerating voltage of 3.0 and 5.0 kV. After the incubation, the cells were harvested and transferred into filtered (0.2 μm sterile syringe filter, Whatman, USA) dechlorinated tap water, to obtain a cell density of $\sim 10^5$ to 10^6 cells per cm^3. Bacteria suspension was then incubated at 37 °C for 5 minutes. Subsequently, C/GO/Al_2O_3/Ag and C/Al_2O_3/Ag nanocomposites were soaked in 200 μl of each suspension of bacteria prepared in tap water and then incubated at 37 °C for 30 minutes. Bacteria to nanomaterial ratio was set as 5×10^{-5} g : 200 cm^3. After this time, 100 μl of 20% (v/v) aqueous glutaraldehyde solution was added to the suspension and the bed was allowed to sediment. After 1 hour, the supernatant was gradually changed to 500 μl of 20, 40, 60, 80, and finally 98% (v/v) ethanol/water solution. Before SEM studies, the obtained samples were dried, deposited onto a sticky carbon tape and coated with a thin carbon layer.

2.7. Analysis of potential antimicrobial properties

2.7.1. Disk diffusion method. The biological activity of the samples was studied using a disk diffusion method against both model and waterborne bacteria strains isolated from the natural environment. The bacterial strains were spread in a form of lines on the surface of Petri dishes with solid nutrient agar (Nutrient LAB-AGAR™, Biocorp). Tested samples were placed directly onto the lines with a respective distance between each other. Such prepared plates were then incubated for 48 hours at 26 °C. Petri dishes were then photographed. The photographs were used for measuring the growth inhibition zones around the exanimated samples. The final result of the growth inhibition zone was calculated as an average from ten repetitions, added with standard deviation.

2.7.2. Filtration process. Based on the results of the disk diffusion test, four bacteria strains were selected for the filtration process. These were two sensitive (*W7* and *W8*) and two resistant (*W6* and *W9*) to developed beds. Immediately before the filtration test, a fresh bacterial suspension was prepared by introducing the appropriate amount of previously selected bacteria into 5 liters of dechlorinated tap water. The number of bacteria (CFUs cm^{-3}) in initial suspension was 7.5×10^5 for fresh hybrid nanocomposites, and 3.0×10^8 for regenerated materials. The samples and pristine activated carbon (used here as a reference) were rinsed with a small amount of distilled water before using in the filtration test. Afterward, they were

introduced into filtration columns in a form of a loosely packed bed of 100 mm high and 10 mm diameter. Then, the previously prepared suspension was introduced to the filtration columns in a 5 cm^3 portion, and the obtained filtrate was collected into measuring vessels. It was essential to ensure that the bed does not dry out or become air locked. The filtrates were collected every 15 minute period, up to 120 minutes. The dilution series were made from each filtrate, and then bacteria were cultured on a standard nutrient agar medium (Nutrient LAB-AGAR™, Biocorp) for 48 hours at 26 °C, using a pour plate technique. The number of bacteria was evaluated using the direct counting method and was calculated as a number of colony forming units (CFU) per 1 cm^3 of water. Measurements of flow velocity (V) were carried out periodically for each of the tested beds. The values were then calculated as a ratio of filtrate volume to the gained time.

2.7.3. Analysis of self-sterilizing properties. To evaluate the ability of the samples to eliminate adsorbed bacteria cells after the filtration process *via* self-sterilization, about 0.5 g of wet filter material was transferred into test tubes with sterile tap water and vigorously shaken. The obtained bacterial suspensions were then cultured using a pour plate technique. Each analysis was repeated after 72 hours of contact time while materials were stored at ambient temperature and in non-sterile conditions.

2.7.4. Regeneration. We have also evaluated the possibility of reusing the filtration bed *via* thermal regeneration. The used bed was subjected to thermal treatment at 105 °C for 24 hours and the filtration process was repeated with the same procedure as described above. The only difference in the procedure was the filtration time, which was reduced to 90 minutes due to the observed bed breakthrough point. Quantitative tests were carried out after 0 and 72 hours of storage at ambient conditions.

3 Results and discussion

3.1. Materials characterization in terms of morphology, structure and potential bioactivity

The obtained C/NCP and C/GO/NCP nanocomposite filtration bed were thoroughly characterized before further evaluation for biological activity. Firstly, we analyzed the morphology of the activated carbon sample (see Fig. 2a) which was used as the carrier for chosen nanomaterials. The SEM images showed a highly porous surface with many longitudinal capillaries. As expected, in the C/NCP nanocomposite, the C pores were filled with NCP (see Fig. 2b) with the presence of ~200 nm Ag nanoparticles (white spots on SEM images). Not surprisingly, the SEM images of the C/GO/NCP filtration bed revealed the presence of GO flakes with micro-scale sizes (see Fig. 2c). We have also observed that NCPs have had a tendency to agglomeration in larger G cavities, but also on the relatively sharp edges of the GO flakes. This effect was also observed in earlier studies on GO/NCPs[21,24,27] and it could be explained by the greater possibility of the attachment of NCP precursor to the exposed area of the GO carrier. This effect could have influenced the porosity.

To quantitatively verify the porosity of samples, we have used physical nitrogen sorption analysis. The obtained results were summarized in Fig. 2d. Results of the specific surface area S_{BET} indicate that C/GO/NCP and C/NCP beds adsorbed relatively more nitrogen in comparison to the reference C sample. The S_{BET} of C/NCP was ~21% and ~5.6% higher when compared with C/GO/NCP and C, respectively. The observed increase in S_{BET} parameter for surface-modified carbon is strongly related to the evolution of surface area caused by the presence of attached nanoparticles.

On the other hand, a slight decrease in S_{BET} of C/GO/NCP and a large decrease of V_{pore} concerning C/NCP bed is caused by the presence of GO/NCP on the surface, which most likely has closed some amount of open pores present in pure C. At a first glance, this effect could result in a decrease in a performance of the filtration bed. However, the true performance could be verified only in a dynamic condition of the filtration process.

After materials characterization, we were not entirely convinced about the expected performance of C/NCP and C/GO/NCP nanocomposite beds in the filtration process. Therefore, we have moved to biological investigations to challenge them with various types of bacteria. This part concentrated on finding the most efficient composition for the filtration bed and further verification of this performance in the model and close-to-real conditions. Firstly, we investigated the antibacterial properties of filtration beds in model conditions. For this purpose, few grains of C/NCP, C/GO/NCP filtration beds, and C (reference sample) were placed directly on agar-filled Petri dishes with linearly cultured bacteria then incubated. After incubation, the viability of model bacteria was calculated (see Fig. 3a) on basis of the growth inhibition zones (shown in Fig. 3b–d). We have noticed that all bacteria exposed to the reference C sample showed 100% viability. The viability was, however, reduced by both C/NCP and C/GO/NCP up to even 100%. The strongest bacteria viability reduction was observed in case of *Bacillus* sp. (92–100%) while *S. aureus* possessed the highest resistance to investigated hybrid nanocomposite (38–45% of viability reduction). It was also noted that the viability of model bacteria strains was 6.5–8% higher for C/GO/NCP filtration bed in comparison to C/NCP.

In the next step of the study, we have investigated the antibacterial properties in close-to-real conditions on waterborne bacteria isolated from natural surface waters. The so-called reduction culturing resulted in obtaining 12 pure bacteria strains, further designated by '*W*' letter.

We carried out the preliminary analysis for the simulated *coccobacillus*/*staphylococci* cells mixture and verified the adsorption properties of beds toward chosen bacteria cells using SEM. The images of the obtained bio-adsorption properties for C/NCP and C/GO/NCP filtration beds were presented in Fig. 4a and b, respectively. We noted that bacteria cells were randomly attached to the surface of both nanocomposites and have created clusters of cells with similar morphologies. The high magnification SEM images revealed both normal and disrupted morphology of various cell types.

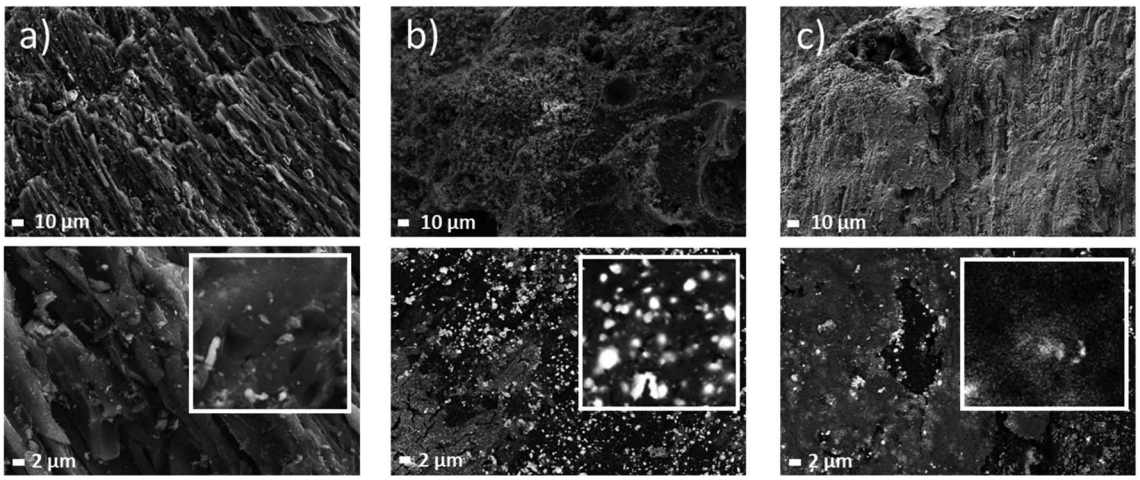

d)

Sample	S_{BET} ($m^2\ g^{-1}$)	S_{pore} ($m^2\ g^{-1}$)	V_{pore} ($cm^3\ g^{-1}$)	D_{pore} (nm)
C	796.6	40.5	0.047	3
$C/Al_2O_3/Ag$	1006.1	96.1	0.107	3
$C/GO/Al_2O_3/Ag$	948.2	89.2	0.099	4

Fig. 2 Characterization of the morphology for (a) granular activated carbon and (b) $C/Al_2O_3/Ag$ (C/NCP) (c) $C/GO/Al_2O_3/Ag$ (C/GO/NCP) hybrid nanocomposite beds. Ag nanoparticles are visible here as bright spots and GO flakes – as light grey areas. (d) Physical properties of the obtained materials such as Brunauer–Emmett–Teller surface area (S_{BET}), pore surface area (S_{pore}), pore volume (V_{pore}), and mean pore size (D_{pore}), obtained using physical nitrogen sorption analysis.

Subsequently, we have moved into the disk diffusion tests which were performed using the same procedure as in the case of model bacteria strains to show the bacteria growth inhibition zones. Images obtained for natural waterborne bacteria in presence of C, C/NCP, and C/GO/NCP hybrid nanocomposite filtration beds were presented in Fig. 4c–e, respectively.

The results showed that W3, 4, 6, and 9 strains exhibited resistance to C/NCP while *W7*, *8*, and *12* strains were most sensitive to tested materials (see Fig. 4d). Also, the introduction of GO did not improve the biological activity of the hybrid nanocomposites. In case of *W12* strain, its presence even lowered the biocidal activity of the beds. It is generally accepted that GO immobilizes bacteria cells mostly due to the aggregation on their cell wall and further damage by sharp-edged nanoflakes.[28–30] However, in case of our nanocomposites, GO flakes more likely acted as an adhesive to C grains (see the SEM images, Fig. 2 b and c) then attached *via* sharp edges.

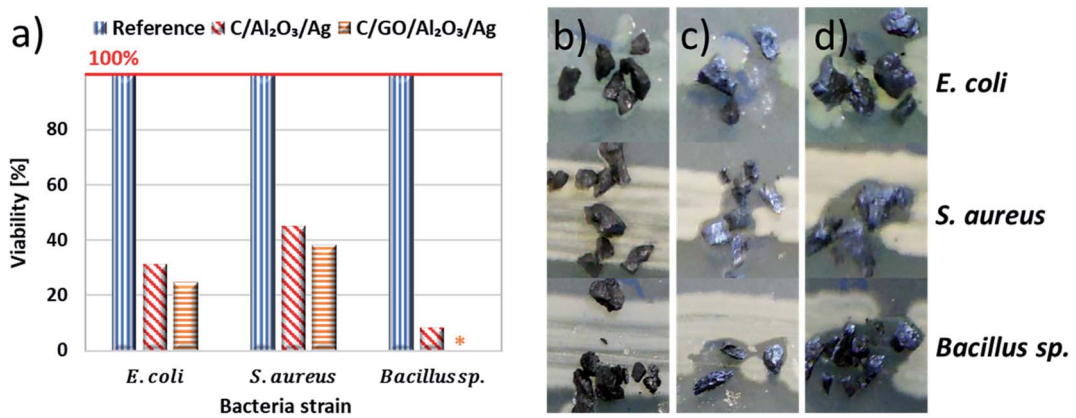

Fig. 3 Characterization of the model biological properties of developed hybrid nanocomposites against selected model bacteria strains. (a) The quantitative assessment of the antibacterial efficiency for developed filtration nanocomposites. Zero viability was marked with an asterisk (*). Photographs of Petri dishes showing growth inhibition zones in presence of the (b) granular activated carbon (C), (c) $C/Al_2O_3/Ag$ (C/NCP) and (d) $C/GO/Al_2O_3/Ag$ (C/GO/NCP) hybrid nanocomposite for *Escherichia coli*, *Staphylococcus aureus* and *Bacillus* sp.

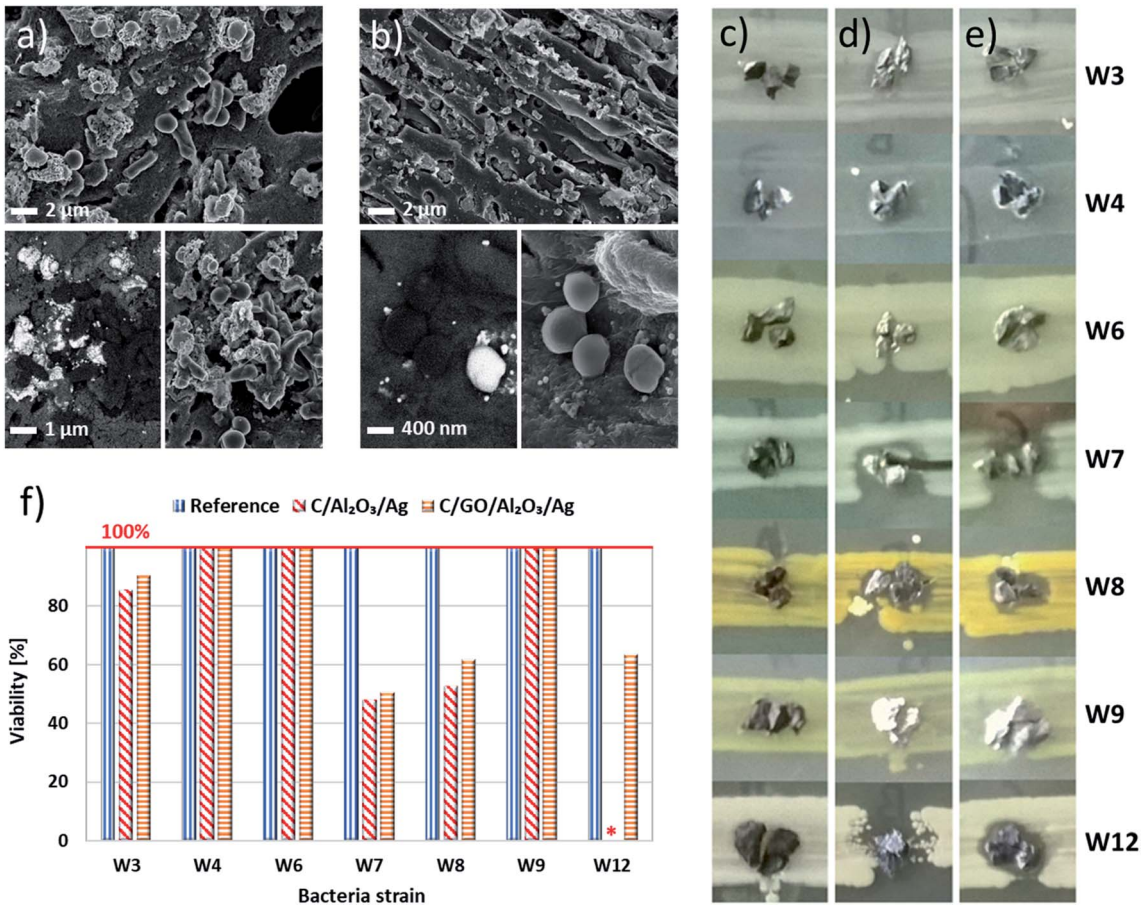

Fig. 4 Characterization of close-to-real biological properties of developed hybrid nanocomposites against selected waterborne bacteria strains isolated from the natural environment. SEM images of bio-adsorption properties of (a) C/Al_2O_3/Ag (C/NCP) and (b) C/GO/Al_2O_3/Ag (C/GO/NCP) nanocomposites carried out in static conditions for simulated *coccobacillus*/*staphylococci* cells mixture. Photographs of Petri dishes showing growth inhibition zones in presence of the (c) granular activated carbon, (d) C/NCP and (e) C/GO/NCP hybrid nanocomposite. (f) The quantitative assessment of the antibacterial efficiency for developed filtration nanocomposites. Zero viability was marked with an asterisk (*).

Next, we analyzed obtained results in terms of reducing bacteria viability. The obtained results were compared quantitatively and presented in Fig. 4f. After taking a brief look, one would notice that granular activated carbon did not disturb the viability of any of the investigated bacteria strains. Viability of *W7*, *W8* and *W12* bacteria were however strongly interrupted by both C/NCs and C/GO/NCP nanocomposite, which reduced it to 48–63%, and even 0% in case of *W12* strain and C/NCP. When an impact of nanocomposite on the tested strains was observed, in 3 out of 4 cases introduction of GO deteriorated the antibacterial effect (about 3–9%). The viability of *W4*, *W6* and *W9* strains was not affected by any of the investigated samples.

We have also noted that the growth inhibition zones around the grains were not uniform, and this may indicate uneven Ag^+ ions diffusion from C/NCP and C/GO/NCP grains into the agar substrate. It should be stressed here that agar tests may not appear fully relevant with non-soluble samples or larger grains, like in our case. Therefore, we made a case that agar tests have given us only preliminary information on the potential bioactivity of designed filtration beds, and we should move into more advanced investigations. The principal rule of the disk diffusion method is that bioactive substance needs to diffuse into an agar base to enable inhibition of bacteria growth. In the case of metallic nanoparticles and nano-oxides, these are mostly metal ions. However, the potential antimicrobial activity is due to the diffusion of their ions after oxidation.[10,13,14,31–36]

To this end, we have obtained enough information on materials properties and their potential bioactivity. However, most credible verification of the performance of filtration beds could be done only in a water-flow system. Therefore, the next part of the study relates to investigations carried out under dynamic conditions. Most importantly, the filtration beds regeneration approach gave the final answer on a real application potential of C/NCP and C/GO/NCP nanocomposite beds.

3.2. Verification of materials' properties in the filtration process and regeneration approach

To finally verify the application potential of the developed hybrid nanocomposite filtration beds, we have carried our water decontamination tests in filtration columns. We filled them with fresh and regenerated C/GO/NCP and C/NCP beds before and after regeneration. The designed filtration system was able

to mimic dynamic water flow conditions during filtration. Therefore, we were also able to check crucial filtration parameter which is the flow velocity (V).

The gentle pouring of the grains enabled the creation of a loosely fixed filtration bed with no damage to the structure of grains. In general, we have shown that modification of C with GO/NCP and NCP slightly increased the flow velocities (V) *i.e.*, maximal (V_{max}), minimal (V_{min}) and average (V_{av}) values in both modification cases (see Fig. 5a). More specifically, the surface modification of C with GO/NCP caused a higher increase of flow velocities in comparison to C/NCP. We suspect this phenomenon may be caused by aggregation of single GO nanoflakes into bigger agglomerates. Gurunathan *et al.*[28] and Liu *et al.*[29] confirmed this tendency. It is worth to note that measured flow velocity values were maintained after the regeneration process, although they decreased slightly in both cases.

To evaluate if the bio-adsorption properties of C/GO/NCP and C/NCP hybrid nanocomposites toward bacteria cells are maintained concerning materials testing in dynamic flow conditions, we carried out a filtration process. The results of bacteria removal obtained as a function of time for fresh and regenerated nanocomposites were presented in Fig. 5b and c, respectively. The C/GO/NCP and C/NCP nanocomposites showed a superior efficiency (near 100%) in eliminating bacteria cells from the filtrated suspension. The fresh C/GO/NCP sample showed slightly better effectiveness over the C/NCP and held over 99% efficiency in bacteria elimination during 120 minutes (see Fig. 5b). The high capability in eliminating the bacteria cells from filtered suspension was also preserved in case of regenerated materials (see Fig. 5c). Due to the nearer breakthrough point, we decided to reduce the filtration time to 90 minutes. Also, in this case, the C/GO/NCP nanocomposite showed slightly lower efficiency then C/NCP. This nanocomposite showed an efficiency of 99.8–99.9% throughout the whole filtration process.

Nevertheless, in case of C/NCP, it was closer to 99.99%. The observed differences are not significant and can be the result of methodology limitations. It is also worth to mention that oxygen functional groups located at edges of GO such as carboxyl, hydroxyl and epoxy, participating in bacterial cell disruption, could be thermally degraded in the regeneration process and may have contributed as well.[28,29,37,38]

Satisfied with the results on bacteria removal during the filtration process, we have moved into verifying of potential concerns about the possibility of secondary contamination. This effect appears in case of filtration beds (mostly carbons) that efficiently remove bacteria but do not reduce their viability.[39,40] The possibility of bacteria settling on the surface of

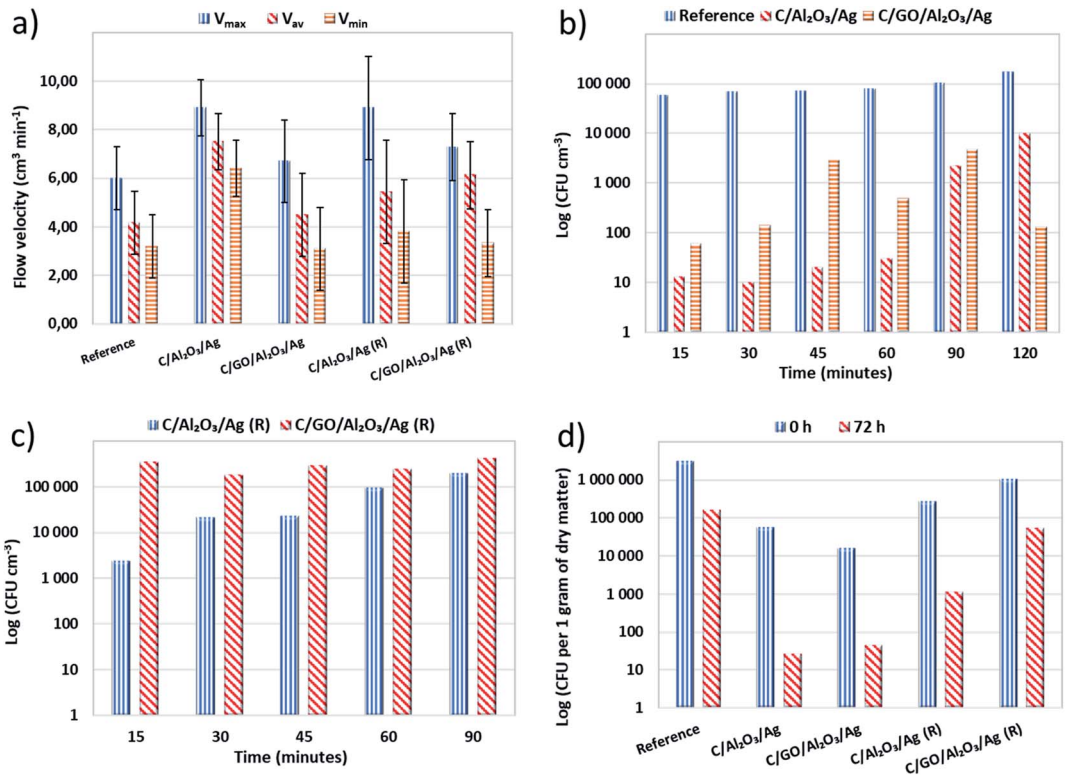

Fig. 5 Results from the filtration process carried out in close-to-real conditions. (a) Maximum (V_{max}), average (V_{av}), and minimum (V_{min}) flow velocities measured during the filtration process for $C/Al_2O_3/Ag$ (C/NCP) and $C/GO/Al_2O_3/Ag$ (C/GO/NCP) filtration nanocomposites in comparison with the reference granular activated carbon (C). The efficiency of the filtration process showing collected bacteria of colony-forming units (CFUs) per cm^3 of (b) fresh and (c) regenerated filtration nanocomposites at each time-point of the process. A number of CFUs per cm^3 for each filtration nanocomposite revealed for filtrates collected at the time of the ongoing filtration process. (d) Number of CFUs per 1 gram of dry matter obtained for fresh and regenerated filtration nanocomposites after 0 and 72 hours of contact time.

filtration beds is being utilized in so called biologically active carbon filter beds.[41] Due to organic matter on the porous surface of activated carbon, it is an excellent source of nutrients and energy for microorganisms. Therefore, it creates a good base for their growth.[42,43] Bacteria living on the surface of activated carbon decompose organic contamination and cause its bio-regeneration.[44] However, we have made the case that potentially pathogenic bacteria may be detached and flushed away with filtrate and for that reason, it creates a severe health safety hazard.[40,45]

The *post mortem* biological tests carried out on nanocomposites after the filtration process unequivocally confirmed the superior activity of the nanocomposites. The percentage efficiency of the filtration process is presented in Fig. 6a. The number of colony forming units (CFUs) per gram of dry matter, obtained for the fresh hybrid nanocomposites and the regenerated samples after 72 hours of contact time are shown in Fig. 6b. We compared the obtained results with the samples taken immediately after the filtration process and then calculated percentage efficiency.

As shown in Fig. 6b, the C sample absorbed a lot of bacterial cells. That is why we have concluded that its bacteria removal efficiency, observed in a filtration process, resulted only from its adsorption capacity. Both C/GO/NCP and C/NCP nanocomposites showed remarkable efficiency in eliminating bacterial cells absorbed on their surface. However, nanocomposite that was not enriched with GO flakes adsorbed almost 3.5 times more bacteria concerning the rest of the samples. Even though both nanocomposites reduced the number of adsorbed cells by the same order of magnitude, C/NCP was revealed to be much more effective (99.99 *vs.* 99.73%, respectively). If it would be due to a lack of nutrients, we should observe similar efficiency for all investigated materials. However, the unmodified C has shown only 95.03% of bacteria deactivation efficiency. This could also partly confirm our earlier assumptions about the reduction of porous space of granular activated carbon by GO nanoflakes. C/NCP hybrid nanocomposite also retained the desired biological activity to a greater extent, as it adsorbed less of bacterial cells and successfully neutralized them after a direct contact time of 72 hours (99.59% of efficiency). The same cannot be said about the nanocomposite modified with GO flakes, for which the efficiency was only 94.92% (less than for granular activated carbon), and the level of bacteria absorption was higher.

Given that in the case of hybrid nanocomposite with RGO we obtained similar or even worse results. One needs to consider if its presence is beneficial or even necessary. Obviously, a key factor for future application, especially for filtration systems of developing countries, might be the cost. Although the RGO price was relatively high initially, over the years, it constantly drops.[46] Secondly, eliminating one of the compounds simplifies the structure of such nanocomposite and, therefore, clarifies the synthesis route. Also, the nanotoxicity of nanocomposites is not just a sum of compounds, and rather a synergic effect is observed. The nanotoxicity of graphene has been noticed in many studies,[47,48] which in total speaks against this compound. However we need, to remember that in the case of photocatalytic nanoparticles, *e.g.*, TiO_2, the presence of RGO may be more than desirable. It was found that RGO can enhance the separation of the electron–hole pairs and inhibit the charge recombination. What is more, RGO supported materials could be driven photocatalytic in visible and near-infrared light. Therefore, superior antibacterial properties of such RGO/photocatalytic NPs which are active in daylight may be observed.[49]

4 Conclusions

Opportunities for nanomaterials used in sustainable water purification technologies attract particular interest due to their proven antibacterial activity, also against many potentially pathogenic strains. Apart from various nanomaterials that are being extensively studied in recent years, development of both effective and sustainable tap water filtration technology remains a challenge. Our study considers multifunctional carbon-supported bioactive hybrid nanocomposite beds for efficient water decontamination from microorganisms. The results have shown that it is possible to design effective

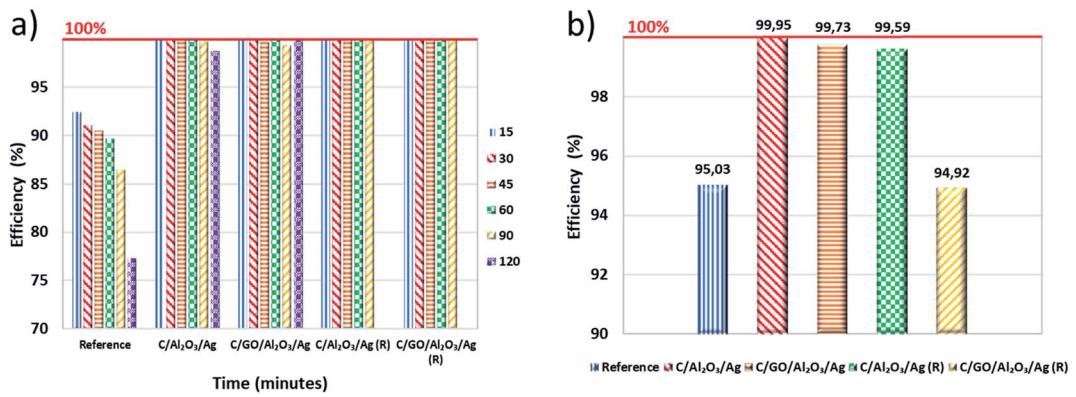

Fig. 6 Percentage efficiency of the filtration process in (a) eliminating and (b) immobilizing bacterial cells (after 72 h of contact time) for fresh and regenerated $C/Al_2O_3/Ag$ (C/NCP), and $C/GO/Al_2O_3/Ag$ (C/GO/NCP) filtration nanocomposites in comparison with the reference granular activated carbon (C).

nanofiltration beds using facile *in situ* surface decoration *via* a sol–gel approach. The obtained nanocomposites were effective against both model bacteria strains, as well as waterborne microorganisms in close-to-real static and dynamic filtration conditions. Introduced bacteria tended to create bigger clusters with the cells of the same morphology and accumulate in thin pores and on the edges of the base material. In static conditions, obtained hybrid nanocomposites were active biologically only against some of the waterborne strains, which was rather due to the diffusion of Ag^+ ions to the agar base, than the adsorption of the cells into the porous structure.

Novel multifunctional carbon-supported bio-active hybrid C/Al_2O_3/Ag (C/NCP) and C/GO/Al_2O_3/Ag (C/GO/NCP) nanocomposites, obtained with zero-waste one-pot technology, showed superior activity against waterborne bacterial strains, which were supported by self-sterilizing properties. The nanocomposites' features include over 99% efficiency in bacteria elimination after 72 hours of contact, water flux maintained at the level of 4.5–7.5 $cm^3\ min^{-1}$ for pristine materials and 5.4–6.1 $cm^3\ min^{-1}$ after regeneration as well as the effectiveness of elimination of bacterial cells of over 99% after regeneration (for 60 minutes of filtration).

We did not notice bacteria resistance in the filtration process. Both of the obtained hybrid nanocomposites showed extraordinary capacity in neutralizing microorganisms' cells in the filtrated suspension, giving almost 100% efficiency throughout the 120 minutes of the ongoing process. Also, the improvement of bioactivity was accompanied by the increase of flow velocity. What is more, we fully or partially recovered the desirable properties of synthesized hybrid nanocomposites using the low-temperature thermal regeneration. The developed hybrid nanocomposite filtration beds were comprehensively verified and compared with the literature data (Table S8.1, see ESI†). On this basis, we conclude that this is the best available solution.

Author contributions

M. J. performed, analyzed and commented on bactericidal analyses and filtration test, collected and analyzed the obtained results, designed and prepared figures, and also prepared and corrected the original manuscript; E. K. designed the concept and content of the experiment, analyzed the obtained results, analyzed and commented on bactericidal analyses, designed figures, coordinated and supervised the preparation of the manuscript as well as coordinated the whole research, A. F prepared and characterized studied samples, carried out bacterial cells adsorption experiment, A. M. J. prepared and characterized studied samples, acquired funds, coordinated and supervised the preparation of the manuscript, corrected the original manuscript and participated in a discussion on obtained results.

Conflicts of interest

There are no conflicts of interest to declare.

Acknowledgements

This research was funded by The National Science Centre, grant 'OPUS 18' number UMO-2019/35/B/ST5/02538. The UST-M Sp. z o.o. Company (Piaskowa 124A, 97-200 Tomaszów Mazowiecki, Poland) is kindly acknowledged for the sample of granular activated carbon for research purposes. M. J. also acknowledges financial support from IDUB project (Scholarship Plus programme).

References

1 N. H. Mthombeni, L. Mpenyana-Monyatsi, M. S. Onyango and M. N. B. Momba, *J. Hazard. Mater.*, 2012, **217–218**, 133–140.
2 I. Sheet, H. Holail, Z. Olama, A. Kabbani and M. Hines, *Int. J. Curr. Microbiol. Appl. Sci.*, 2013, **2**, 1–11.
3 World Health Organization (WHO), *Sanitation and Hygiene: 2017 Update and SDG Baselines*, https://www.unicef.org/publications/index_96611.html, accessed 10 January 2021.
4 T. Q. Tuan, N. Van Son, H. T. K. Dung, N. H. Luong, B. T. Thuy, N. T. Van Anh, N. D. Hoa and N. H. Hai, *J. Hazard. Mater.*, 2011, **192**, 1321–1329.
5 Q. Li, S. Mahendra, D. Y. Lyon, L. Brunet, M. V. Liga, D. Li and P. J. J. Alvarez, *Water Res.*, 2008, **42**, 4591–4602.
6 N. T. Phuong Phong, N. V. Ke Thanh and P. H. Phuong, *J. Phys. Conf. Ser.*, 2009, **187**, 012079.
7 F. Heidarpour, W. Wan Ab Karim Ghani, F.-R. Ahmadun, S. Sobri, M. Zargar and M. Mozafari, *Dig. J. Nanomater. Biostructures*, 2010, **5**, 797–804.
8 L. R. Pokhrel, R. Dean, Z. L. Jacobs and W. B. Burrows, *Nanotechnol. Charact. Tools Environ. Heal. Saf.*, 2019, 1–353.
9 T. Masciangioli and W. X. Zhang, *Environ. Sci. Technol.*, 2003, **37**, 102–108.
10 M. J. Hajipour, K. M. Fromm, A. Akbar Ashkarran, D. Jimenez de Aberasturi, I. R. de Larramendi, T. Rojo, V. Serpooshan, W. J. Parak and M. Mahmoudi, *Trends Biotechnol.*, 2012, **30**, 499–511.
11 M. A. Shahbazi, M. Hamidi, E. M. Mäkilä, H. Zhang, P. V. Almeida, M. Kaasalainen, J. J. Salonen, J. T. Hirvonen and H. A. Santos, *Biomaterials*, 2013, **34**, 7776–7789.
12 M. A. Gatoo, S. Naseem, M. Y. Arfat, A. Mahmood Dar, K. Qasim and S. Zubair, *Biomed Res. Int.*, 2014, **2014**, 1–8.
13 P. K. Stoimenov, R. L. Klinger, G. L. Marchin and K. J. Klabunde, *Langmuir*, 2002, **18**, 6679–6686.
14 S. Silver, L. T. Phung and G. Silver, *J. Ind. Microbiol. Biotechnol.*, 2006, **33**, 627–634.
15 H. Marsh and F. Rodríguez-Reinoso, *Activated Carbon*, Elsevier Inc., 2006.
16 A. Bhatnagar, W. Hogland, M. Marques and M. Sillanpää, *Chem. Eng. J.*, 2013, **219**, 499–511.
17 R. Bandyopadhyaya, M. V. Sivaiah and P. A. Shankar, *J. Chem. Technol. Biotechnol.*, 2008, **83**, 1177–1180.
18 N. R. Srinivasan, P. A. Shankar and R. Bandyopadhyaya, *Carbon*, 2013, **57**, 1–10.
19 H. Zhang and V. Oyanedel-Craver, *J. Hazard. Mater.*, 2013, **260**, 272–277.

20 L. Mpenyana-Monyatsi, N. H. Mthombeni, M. S. Onyango and M. N. B. Momba, *Int. J. Environ. Res. Public Health*, 2012, **9**, 244–271.
21 A. M. Jastrzębska, J. Karcz, E. Karwowska, A. Fiedorczuk and A. Olszyna, *Int. J. Appl. Ceram. Technol.*, 2016, **13**, 856–870.
22 A. M. Jastrzębska, J. Karcz, E. Karwowska and A. Olszyna, *J. Alloys Compd.*, 2017, **724**, 869–878.
23 A. Jastrz□bska, A. Derecka, E. Karwowska, A. Pląsek, T. Wojciechowski, W. Ziemkowska and A. Olszyna, *J. Nano Res.*, 2017, **47**, 89–95.
24 A. M. Jastrz□bska, J. Jureczko, J. Karcz, A. Kunicki, W. Ziemkowska and A. Olszyna, *Chem. Pap.*, 2017, **71**, 579–595.
25 A. M. Jastrzębska, J. Karcz, R. Letmanowski, D. Zabost, E. Ciecierska, J. Zdunek, E. Karwowska, M. Siekierski, A. Olszyna and A. Kunicki, *Appl. Surf. Sci.*, 2016, **362**, 577–594.
26 A. M. Jastrzębska, J. Karcz, E. Karwowska and A. Olszyna, *J. Alloys Compd.*, 2017, **724**, 869–878.
27 A. M. Jastrzebska, J. Karcz, R. Letmanowski, D. Zabost, E. Ciecierska, M. Siekierski and A. Olszyna, *J. Alloys Compd.*, 2016, **679**, 470–484.
28 S. Gurunathan, J. W. Han, A. Abdal Dayem, V. Eppakayala and J. H. Kim, *Int. J. Nanomedicine*, 2012, **7**, 5901–5914.
29 S. Liu, T. H. Zeng, M. Hofmann, E. Burcombe, J. Wei, R. Jiang, J. Kong and Y. Chen, *ACS Nano*, 2011, **5**, 6971–6980.
30 O. Akhavan and E. Ghaderi, *ACS Nano*, 2010, **4**, 5731–5736.
31 M. A. Ansari, H. M. Khan, A. A. Khan, S. S. Cameotra, Q. Saquib and J. Musarrat, *J. Appl. Microbiol.*, 2014, **116**, 772–783.
32 W. Jiang, H. Mashayekhi and B. Xing, *Environ. Pollut.*, 2009, **157**, 1619–1625.
33 A. Mukherjee, I. Mohammed Sadiq, T. C. Prathna and N. Chandrasekaran, *Sci. against Microb. Pathog. Commun. Curr. Res. Technol. Adv.*, 2011, 245–251.
34 L. K. Ruddaraju, P. N. V. K. Pallela, S. V. N. Pammi, V. S. Padavala and V. R. M. Kolapalli, *Mater. Sci. Semicond. Process.*, 2019, **100**, 301–309.
35 Z. Kanwal, M. A. Raza, S. Riaz, S. Manzoor, A. Tayyeb, I. Sajid and S. Naseem, *R. Soc. Open Sci.*, 2019, **6**, 1–15.
36 A. Roy, B. S. Butola and M. Joshi, *Appl. Clay Sci.*, 2017, **146**, 278–285.
37 L. Song, F. Khoerunnisa, W. Gao, W. Dou, T. Hayashi, K. Kaneko, M. Endo and P. M. Ajayan, *Carbon*, 2013, **52**, 608–612.
38 A. Olborska, A. Janas-Naze, Ł. Kaczmarek, T. Warga and D. S. Che Halin, *Autex Res. J.*, 2020, **20**, 506–516.
39 C. Wallis, C. H. Stagg and J. L. Melnick, *Water Res.*, 1974, **8**, 111–113.
40 J. V. Fiore and R. A. Babineau, *Appl. Environ. Microbiol.*, 1977, **34**, 541–546.
41 M. D. Matovic, *Biomass Now: Cultivation and Utilization*, IntechOpen, 2013.
42 H. Sarma and W. Y. Lee, *Environ. Sci. Pollut. Res.*, 2018, **25**, 17227–17239.
43 E. S. Fonte, A. M. Amado, F. Meirelles-Pereira, F. A. Esteves, A. S. Rosado and V. F. Farjalla, *Microb. Ecol.*, 2013, **66**, 871–878.
44 G. M. Walker and L. R. Weatherley, *Process Saf. Environ. Prot.*, 1998, **76**, 177–182.
45 K. D. Pandey, A. K. Patel, M. Singh, Vandana, A. Kumari and Jalaluddin, *Secondary metabolites from bacteria and viruses*, Elsevier Inc., 2021.
46 Graphenea, *The Price Of Graphene*, https://www.graphenea.com/pages/graphene-price#.YJFeZ4ZMRPY, accessed 08 May 2021.
47 A. M. Jastrzębska and A. R. Olszyna, *J. Nanoparticle Res.*, 2015, **40**, 1–21, DOI: 10.1007/s11051-014-2817-0.
48 A. M. Jastrzębska, P. Kurtycz and A. R. Olszyna, *J. Nanoparticle Res.*, 2012, **14**, 12, DOI: 10.1007/s11051-012-1320-8.
49 Y. S. Chen, B. K. Chao, T. Nagao and C. H. Hsueh, *Mater. Chem. Phys.*, 2020, **240**, 122216.